American Mineralogist, Volume 97, pages 419–424, 2012

Spectroscopic characterization of alkali-metal exchanged natrolites

Dan Liu,[1] Zhenxian Liu,[2] Yongmoon Lee,[1] Donghoon Seoung,[1] and Yongjae Lee[1,*]

[1]Department of Earth System Sciences, Yonsei University, Seoul 120-749, Korea
[2]Geophysical Laboratory, Carnegie Institution of Washington, Washington, D.C. 20015, U.S.A.

Abstract

Synchrotron infrared (IR) and micro-Raman spectroscopic studies have been performed on zeolite natrolites as a function of the non-framework composition at ambient conditions. This establishes the spectroscopic characterization of the ion-exchanged natrolites in the alkali-metal series both in the as-prepared hydrated (M-NAT-hyd, M = Li, Na, K, Rb, and Cs) and some stable dehydrated forms (M-NAT-deh, M = Rb and Cs). The former series exhibits non-framework cation-size dependent opening of the helical channels to span ca. 21° range in terms of the chain rotation angle, ψ (or ca. 45° range in terms of the chain bridging angle, T-O2-T). For these hydrated phases, both IR and Raman spectra reveal that the degree of the red-shifts in the frequencies of the helical 8-ring channel as well as the 4-ring unit is proportional to the ionic radius of the non-framework cations. Linear fits to the data show negative slopes of –55.7 from Raman and –18.3 from IR in the 8-ring frequencies and ionic radius relationship. The spectroscopic data are also used to identify the modes of the dehydration-induced "collapse" of the helical 8-ring channels as observed in the stable anhydrous Rb-NAT-deh and Cs-NAT-deh. In addition, we demonstrate that the spectroscopic data in the hydrated series can be used to distinguish different water arrangements along the helical channels based on the frequency shifts in the H-O-H bending band and the changes in the O-H stretching vibration modes.

Keywords: Natrolite, alkali-metal exchange, micro-Raman spectroscopy, synchrotron infrared spectroscopy

Introduction

The structural and chemical diversity of zeolitic minerals originates from dozens of different framework types and their selectivity toward non-framework species. Identifying individual framework structural units and their interactions with specific non-framework species is therefore crucial to understand the thermodynamic stability and properties of natural zeolites. Spectroscopic methods such as IR absorption and Raman scattering have been extensively employed to characterize the interactions between the framework and non-framework components in various natural zeolites (Flanigen et al. 1974; De Man and van Santen 1992). In the case of mineral natrolite, which has been known to be an exclusively sodium-form in the natrolite group zeolites, Pechar and Rykl (1983) first calculated the framework vibrational modes, while mid-IR vibrational modes were obtained by Gottardi and Galli (1985). Later, studies by Goryainov and coworkers revised the mode assignments based on polarized Raman and IR spectroscopy as well as lattice dynamics calculations (Goryainov et al. 2000; Goryainov and Smirnov 2001). The interactions between the non-framework water molecules and the natrolite framework have also been investigated using various combinations of spectroscopic methods and calculations (Boutin et al. 1964; Gunter and Ribbe 1993; Goryainov and Belitsky 1995; Line and Kearly 1998). Recently, Kolesov and Geiger (2006) reported the dehydration behavior of natrolite by in situ high-temperature Raman measurements. They observed that all the O-H bands become gradually broader and weaker with increasing temperature up to 570 K. On the other hand, the effect of the increase in the structural water content during the formation of the ordered-paranatrolite and superhydrated natrolite under hydrostatic pressure has been studied using Raman and IR methods (Demontis et al. 2005; Liu et al. 2010).

We have recently reported that the sodium form of natural natrolite can be exchanged to various alkali-metal cation forms in the K-Rb-Cs series in the hydrated states, which induces successive channel widening by up to 18.5% in terms of the unit-cell volume increase (Lee et al. 2010). Our structural characterizations based on synchrotron X-ray powder diffraction (XRD) and Rietveld refinements also revealed that the arrangements of the non-framework cations and water molecules in the K-, Rb-, and Cs-exchanged natrolites differ significantly from that of the original Na-natrolite. Intriguingly, while the distribution of the non-framework cations becomes similar to one another upon dehydration at elevated temperatures, only the Rb- and Cs-forms "remain" anhydrous upon exposure to atmosphere at ambient conditions (Lee et al. 2011). To shed light into understanding the framework stability as a function of the arrangement of non-framework species, we have carried out a comprehensive spectroscopic investigation using synchrotron IR and micro-Raman spectroscopy on the alkali-metal exchanged natrolites both in the hydrated and stable dehydrated forms.

Experimental methods

The preparation and structural characterization of the alkali-metal exchanged natrolites are described elsewhere (Lee et al. 2010, 2011). The as-prepared ion-exchanged natrolites are in the hydrated forms, M-NAT-hyd (M = Li, Na, K, Rb, and Cs), and for the preparation of the apparently stable anhydrous phases, Rb-NAT-hyd and Cs-NAT-hyd have been heated up to 200 °C in a dry oven over a few hours and quenched to ambient conditions (thereafter named Rb-NAT-deh and

* E-mail: yongjaelee@yonsei.ac.kr

0003-004X/12/0203–419$05.00/DOI: http://dx.doi.org/10.2138/am.2012.3932

Cs-NAT-deh, respectively). The structural models of Na-NAT-hyd, K-NAT-hyd, and Rb-NAT-deh are shown in Figure 1 along with illustrations of the framework building units of natrolite.

Synchrotron IR experiments were performed at the U2A beamline of the National Synchrotron Light Source (NSLS), Brookhaven National Laboratory (BNL). The far-IR spectra were obtained with a Brucker IFS 66v/S Fourier transform infrared (FTIR) spectrometer in combination with a custom-made vacuum microscope system equipped with a Si bolometer detector (Infrared Laboratories) and a 3.5 μm thick Mylar beamsplitter. More details on the optical layout of the beamline have been described elsewhere (Liu et al. 2002). The mid-IR spectra were then collected in transmission mode with a Bruker Vertex 80v FTIR spectrometer and a Hyperion 2000 IR microscope with a nitrogen-cooled MCT detector at the U2A side station. The spectra were collected in the range of 100–700 cm^{-1} for the far-IR and 650–5000 cm^{-1} for the mid-IR. A spectral resolution of 4 cm^{-1} was applied to all measurements. Pure samples were placed between the anvils and comprressed to a few micrometers thickness. The Raman scattering measurements were carried out using a custom-made micro-Raman system at Yonsei University. A Diode-Pumped Solid State (DPSS) laser (Spectra Physics Excelsior CW laser with 532 nm and 150 mW) was used in back-scattering geometry. The laser power on the sample was kept at 15 mW. The average acquisition time for a single spectrum was about 60 s. Raman spectra were measured on M-NAT-hyd (M = Li, Na, and K) samples and are shown in Figure 2. Synchrotron far- and mid-IR spectra were measured on M-NAT-hyd (M = Li, Na, K, Rb, and Cs) and M-NAT-deh (M = Rb and Cs) samples and are shown in Figure 3. Each spectrum was normalized to the strongest band. The peak positions of all the observed IR vibrational modes in this study are compiled in Table 1.

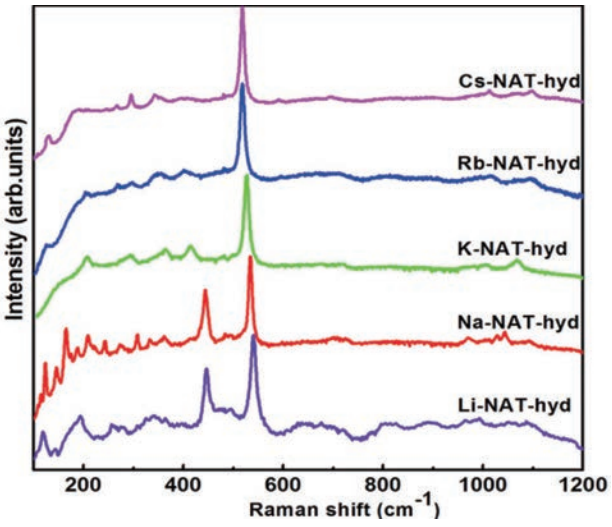

Figure 2. Raman spectra of the hydrated alkali-metal exchanged natrolites at ambient condition. (Color online.)

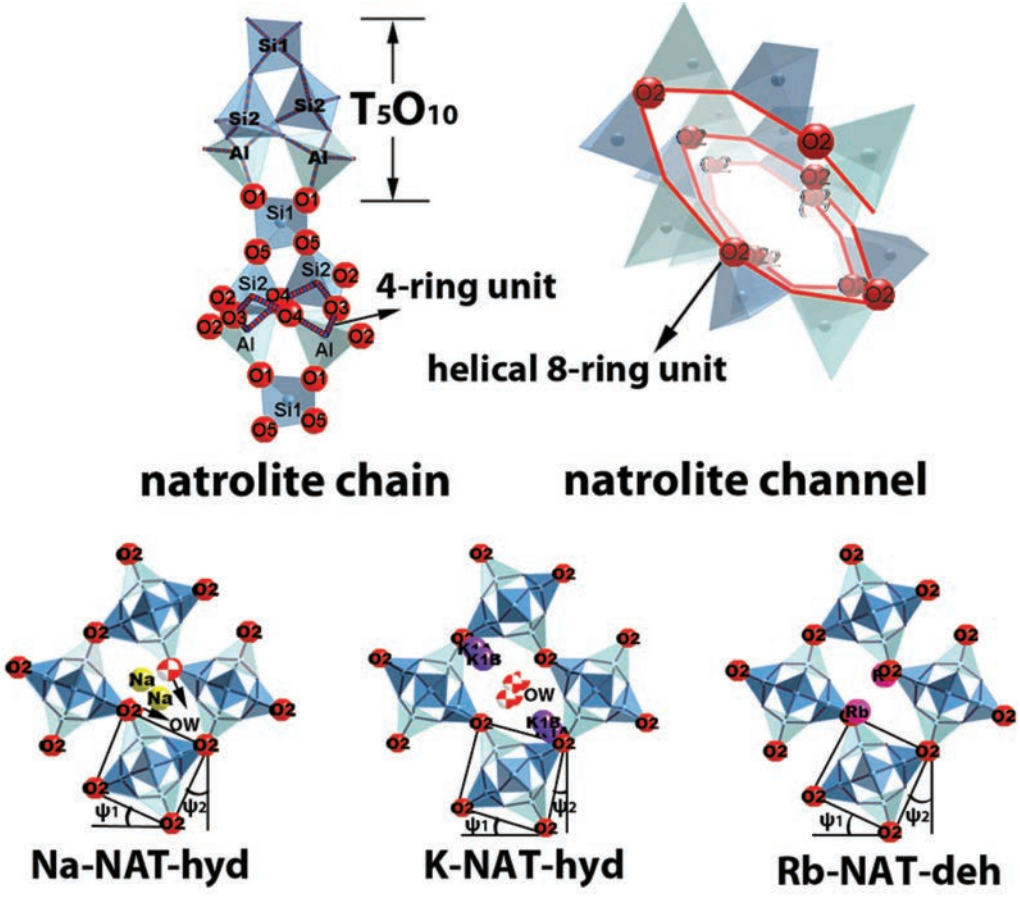

Figure 1. Polyhedral representations of the structural building units of the natrolite framework (**upper**). Some of the tetrahedral vertices are labeled with the bridging oxygen atoms. The 4-ring and helical 8-ring units are emphasized with bold outlines. Structural models of Na-NAT-hyd, K-NAT-hyd, and Rb-NAT-deh are shown **below**. Non-framework cations, water molecular oxygen atoms, and the chain bridging O2 atoms are shown in colored balls. The chain rotation angle, ψ, is outlined with straight lines. (Color online.)

TABLE 1. The peak positions of all the observed far- and mid-IR vibrational modes of different alkali metal-exchanged natrolite at ambient condition

Pechar et al. ν (cm^{-1})	Li-NAT-hyd ν (cm^{-1})	Na-NAT-hyd ν (cm^{-1})	K-NAT-hyd ν (cm^{-1})	Rb-NAT-hyd ν (cm^{-1})	Cs-NAT-hyd ν (cm^{-1})	Rb-NAT-deh ν (cm^{-1})	Cs-NAT-deh ν (cm^{-1})
Translation and libration vibration modes							
110	114.4	107.9	127.2	128.7	128.0	128.7	128.3
130	139.2	136.3	135.8	136.7	136.1	136.3	135.0
136	149.7	144.9	147.1	147.4	148.6	148.0	148.2
168	165.5	163.4	161.1	160.6	162.2	162.5	162.2
			170.4	171.0	171.4	171.4	171.2
186	188.6	183.8	185.5	185.9	184.9	185.9	186.3
			198.4	197.0	196.3	196.7	198.8
218	210.2	207.9	209.3	209.2	208.8	209.3	209.7
220	222.3	220.2	222.5	223.4	223.0	222.5	224.0
228			236.1	235.6	236.7	225.8	236.0
		242.4	247.0	246.3	248.4	247.1	246.7
264		264.7	259.8	259.8	259.8		258.7
278		278.9	278.8	276.1	276.0	275.7	275.3
	290.1	291.2	305.3	300.8	295.4	302.0	297.6
330	323.8	329.5	322.4	321.7	320.1	320.9	320.2
	340.0						
O-T-O bending vibrations of SiO_4 and AlO_4							
365	365.4	363.2	354.4	352.4	349.3	355.5	350.8
			377.8	379.5	370.5	375.4	372.1
420	426.2	422.0	428.9	422.3	413.0	420.7	415.2
440	457.9	442.7		432.5	425.2	434.9	428.0
Libration vibration of the H_2O							
480	494.5	484.9		493.4	494.7	496.0	499.6
510		507.6	500.8	501.8		503.4	
545		545.6	545.0	535.5			
580		579.5	581.9	575.3	568.4	576.0	568.4
T-O stretching vibrations of SiO_4 and AlO_4							
605	617.8	605.6		613.1	601.8	615.0	605.2
625	630.2	627.2	636.5	626.4	627.8	630.2	628.8
				648.1	637.9	649.1	637.2
680	671.9	679.0	672.7	672.8	669.0	675.0	667.9
	699.4	697.1	700.5			683.6	
720	716.2	719.7	715.8			712.0	718.0
	739.8		752.7			761.2	751.6
						952.0	965.1
975	964.1	963.0	963.9	972.7	968.8	978.0	
	993.1	990.0	993.0	993.0	991.4		984.6
	1016.6	1000.2			1020.4	1000.3	1004.2
1055		1047.0	1026.6	1025.0		1030.3	1039.3
	1046.3	1055.9				1046.5	1054.3
	1093.5	1086.0	1064.0	1075.0	1065.3		1094.6
H-O-H bending vibrations of H_2O molecule							
1625	1637.0	1631.5	1620.7	1649.0	1660.0		
***v*O-H stretching vibrations of H_2O molecule**							
3310–3515	3338.0	3322.0	3478.6	3294.3	3286.0		
	3546.8	3538.0	3578.9	3443.2	3424.3		
				3548.4	3463.1		

Note: The relative error of the measured peak position should not exceed 0.1 cm^{-1}.

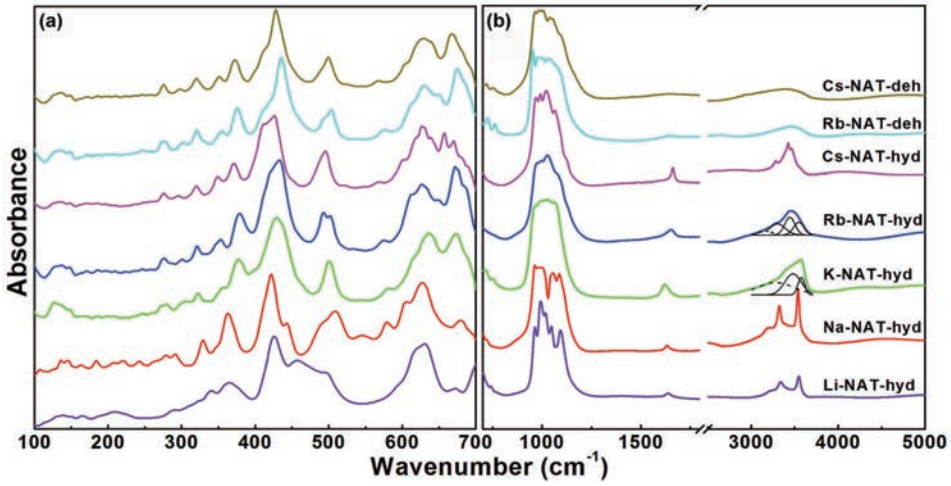

FIGURE 3. (**a**) Far-infrared and (**b**) mid-infrared spectra of the hydrated alkali-metal exchanged natrolites and dehydrated Rb- and Cs-phases at ambient condition. The black curves near 3500 cm^{-1} are the Lorentzian function fits to the broad O-H stretching vibrational bands in K-NAT-hyd and Rb-NAT-hyd. (Color online.)

Results and discussion

The basic structural building unit of the natrolite framework is T_5O_{10} tetrahedra ($Al_2Si_3O_{10}$ or 4=1 unit by International Zeolite Association code). These units are connected along the **c**-axis to form the so-called fibrous chains, which are then interconnected via Al-O-Si linkages by shifting the heights of the chains relative to one another by a quarter of the **c**-axis length (Fig. 1). As a result, helical 8-ring channels are formed in elliptical shape along the **c**-axis, where sodium cations and water molecules are distributed in interpenetrated zigzag chains in a 1:1 ratio to lead to the idealized unit-cell composition of $Na_{16}Al_{16}Si_{24}O_{80}{\cdot}16H_2O$ in space group *Fdd*2 (Meier 1960). The ellipticity of the helical 8-ring channel can be described quantitatively by a chain rotation angle, ψ, which measures the average angle between the sides of the quadrilateral around the T_5O_{10} building unit and the **a**- and **b**-unit-cell axes (Baur et al. 1990). The smaller the ψ angle, the more circular the helical 8-ring channel becomes hence the access to the channel becomes easier. Under ambient conditions, the hydrated sodium natrolite show ca. 24° in ψ, and we have reported that the ψ angle can be systematically reduced to ca. 3° via larger alkali-metal cation substitution (Lee et al. 2010). Once dehydrated, however, the chain rotation angle increases back and the channels "collapse" to more elliptical shapes (Lee et al. 2011). It was also found that the extent of the channel "collapse" after dehydration becomes progressively larger as a function of the non-framework cation size: ψ increases from 12.8 to 28.0° in K-NAT-hyd, from 6.7 to 25.1° in Rb-NAT-hyd, and from 2.9 to 21.6° in Cs-NAT-hyd (Lee et al. 2011). The pore opening size in the dehydrated phases, however, still remains proportional to the size of the alkali-metal cation, and the dehydration of Rb- and Cs-NAT is observed to be irreversible (Lee et al. 2011).

Based on the group theoretical analysis, the phonons in natrolite can be classified to $24A_1 + 25A_2 + 25B_1 + 25B_2$ irreducible representations (Goryainov et al. 2000). Among these 99 predicted optical modes, 57 modes are observable in Raman and IR spectra. The lattice vibrational modes of all the ion-exchanged natrolites studied here are found to exhibit overall similar Raman and IR spectra to that of the original sodium natrolite due to the fact that the framework connectivity remains the same in the space group *Fdd*2 (Figs. 2 and 3). The subtle differences in the observed spectra would then represent the differences in the degree of the framework distortion and cation-water distribution due to the ion-exchange and/or dehydration.

Our data for the original hydrated sodium-natrolite (Na-NAT-hyd) at ambient condition are in good agreement with those reported in the literature (Pechar and Rykl 1983; Line and Kearly 1998). The observed far-IR active modes below 340 cm^{-1} can be assigned to the translational modes of water molecules and the optical mode of the lattice. Similarly, the Raman active modes observed below 420 cm^{-1} are assigned to optical modes of the lattice vibrations. The bands of the O-T-O intra-tetrahedral bending mode are seen in the far-IR region between 410 and 445 cm^{-1} (which correspond to the Raman bands in the range of 420–900 cm^{-1}). The two most intense IR bands located at 610–700 cm^{-1} and 900–1320 cm^{-1} represent the tetrahedral T-O stretching vibrations in the symmetric stretching region (far-IR) and the anti-symmetric stretching region (mid-IR), respectively (Figs. 3a and 3b). One of the most characteristic vibrational modes of the natrolite framework, however, would be the so-called breathing vibrational mode of the helical 8-ring channel as observed previously at 363.2 cm^{-1} in IR and 443 cm^{-1} in Raman for Na-NAT-hyd (Breck 1974; Pechar and Rykl 1983). This band is found to be sensitive to the changes in the T-O2-T chain bridging angle and can therefore be used as a measure of the "elliptical channel-opening" as a function of different cation-water distribution in natrolite (Fig. 1). In accordance to the previous structural studies (Lee et al. 2010, 2011), we find a systematic red-shift of the 8-ring vibrational mode in both IR and Raman active modes as a function of the ionic radius in the M-NAT-hyd series (M = Li, Na, K, Rb, and Cs) (Fig. 4), i.e., the frequency of this band shifts progressively to lower values as the size of the non-framework cation increases. The frequency decrease is by 3 cm^{-1} (IR) and 2.4 cm^{-1} (Raman) from Li- to Na-NAT-hyd, 19 cm^{-1} (IR) and 8.8 cm^{-1} (Raman) from Na- to K-NAT-hyd, 10 cm^{-1} (IR) and 2.0

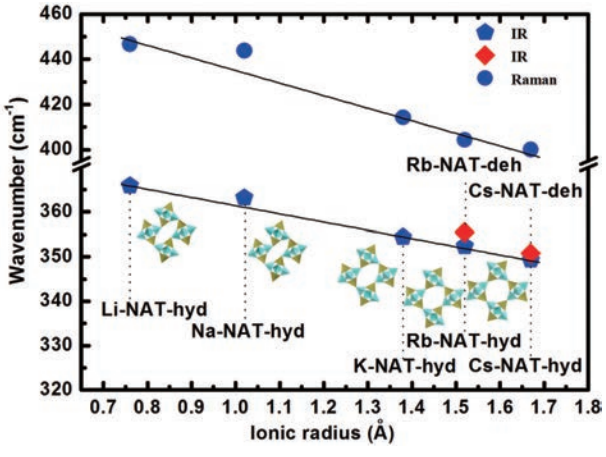

Figure 4. Dependency of the helical 8-ring vibrational modes on the non-framework cation radius. Inset figures illustrate the progressive "pore opening" observed from Li- to Cs-exchanged natrolites. Here, non-framework cations and water molecules are omitted for clarity. The black solid lines are linear fits to the data. (Color online.)

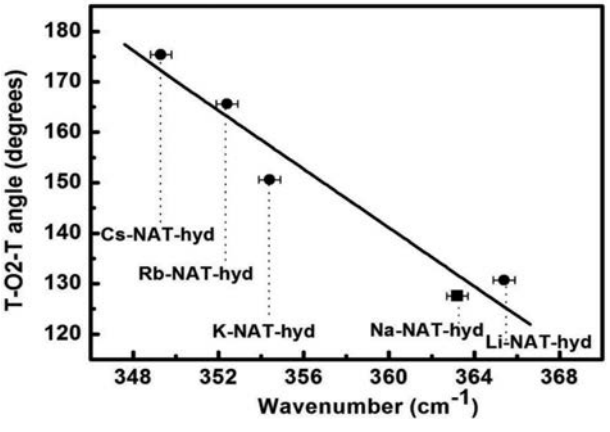

Figure 5. Dependency of the helical 8-ring vibrational modes on the T-O2-T bridging angles. The T-O2-T angles are from the previous crystallographic studies [solid squares from Baur et al. (1990) and solid circles from Lee et al. (2010)].

cm^{-1} (Raman) from K- to Rb-NAT-hyd, and 4.3 cm^{-1} (IR) and 3.1 cm^{-1} (Raman) from Rb- to Cs-NAT-hyd. The "collapse" of the channel-opening upon the loss of water molecules is then observed as the peak shifts back to higher frequencies by 3.1 cm^{-1} (IR) and 1.5 cm^{-1} (IR) from Rb-NAT-hyd to Rb-NAT-deh and from Cs-NAT-hyd to Cs-NAT-deh, respectively. The black solid lines in Figure 4 correspond to linear least-squares fits to the observed frequencies of the helical 8-ring modes vs. respective cation radius in the hydrated forms. The slopes of the lines are –55.7 for Raman and –18.3 for IR. The position of the helical 8-ring vibrational mode can, therefore, be quantitatively related to the degree of the elliptical channel-opening, e.g., the chain rotation angle ψ or the chain bridging angle T-O2-T in the M-NAT-hyd series (Fig. 5). There is an additional prominent band in the range of 370–379 cm^{-1} in the spectra of the hydrated natrolites exchanged with cations larger than sodium, i.e., K-, Rb-, and Cs-NAT-hyd (Fig. 3a). This band might be attributed to the difference in the distribution pattern of the alkali-metal cations and water molecules along the helical 8-ring channels. According to the previously established structural models on Li- and Na-NAT-hyd (Baur et al. 1990), the cations and water molecules are located near the center and the walls of the elliptical channels' minor axes, respectively (Fig. 1). This distribution pattern is reversed in K-, Rb-, and Cs-NAT-hyd, and the cations are located close to the walls of the elliptical channels' major axes and the water molecules near the centers (Fig. 1). This gives rise to the change in the crystal field to induce the new vibration mode.

All of the measured Raman spectra are also characterized by the presence of a strong band in the frequency range between 528 and 518 cm^{-1} (Fig. 2). This band has been assigned to the breathing mode of the 4-ring tetrahedral building unit (Fig. 1). Based on the measured Raman frequencies of the 4-ring units in several synthetic zeolites (Cs-D, Na-X, Li-A, Na-A, Na-P, K-R, and synthetic magadiite), Dutta et al. proposed a linear relationship between the average T-O-T bridging angle of the 4-ring unit and its breathing frequency, i.e., they reported that zeolites having a 4-ring unit feature $\partial v/\partial a$ = 5–6 cm^{-1}/° relationship where v is the frequency in cm^{-1} and a is the average T-O-T bridging angle of the 4-ring in degree (Dutta et al. 1988). For those hydrated ion-exchanged natrolites, the Raman frequency of the 4-ring breathing mode is plotted against the average T-O-T bridging angle of the 4-ring unit in Figure 6. The linear fit to the data gives $\partial v/\partial a \approx 6.4$ cm^{-1}/°, which suggests that the frequency-angle relationship is overall confirmed in natrolites in the hydrated alkali-metal series.

It is a well-known fact that infrared spectroscopy is one of the most sensitive tools to directly observe guest constituents such as H_2O in zeolites via the O-H bending and stretching vibration modes (Kolesov and Geiger 2006). In addition, there exists such a correlation between the frequency of the H-O-H bending band and the H-O-H bond angle that spectroscopically observed H-O-H bending bands can be used to estimate the H-O-H bond angles, which cannot be derived directly from X-ray structural model (Artioli et al. 1984; Kvick et al. 1985; Kolesov and Geiger 2006). The characteristic IR absorption bands from water molecules in M-NAT-hyd series (M = Li, Na, K, Rb, and Cs) are observed in the 1600–1660 cm^{-1} region for the H-O-H bending mode and at around 3400 cm^{-1} for the O-H stretching

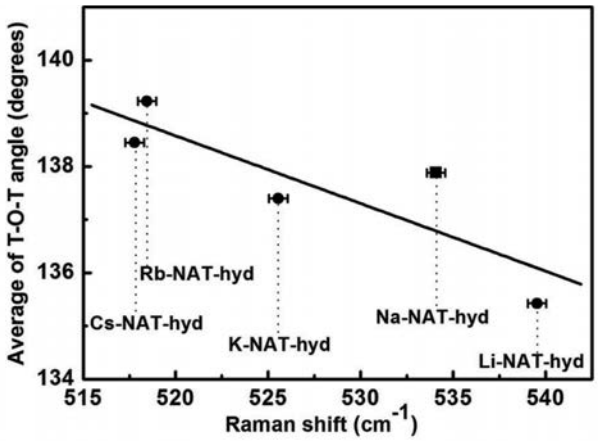

FIGURE 6. Dependency of the 4-ring breathing mode on the average T-O-T bridging angle of the 4-ring unit (avg. between T-O1-T, T-O3-T, T-O4-T, and T-O5-T). The T-O-T angles are from the previous crystallographic studies [solid squares from Baur et al. (1990) and solid circles from Lee et al. (2010)].

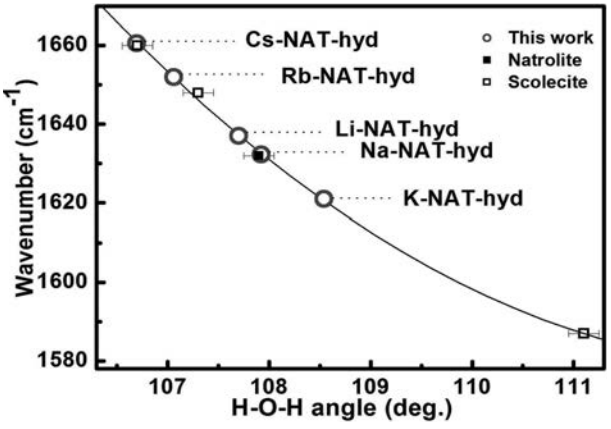

FIGURE 7. Dependency of the H_2O bending mode on the H-O-H angle in the hydrated alkali-metal exchanged natrolites at ambient condition. The curve is the fit to the natrolite and scolecite data by Kolesov et al. (2006).

modes (Fig. 3b). The observed H-O-H bending mode from Na-NAT-hyd is at the same frequency as to that of Kolesov's value from mineral natrolite (Fig. 7). This implies that the H-O-H bending frequencies from the other cation forms can be used to estimate their respective H-O-H angles (Fig. 7). We observe a gradual increase in the frequency of the H-O-H bending band from 1632 to 1661 cm^{-1} with increasing non-framework cation size for Na-, Rb-, and Cs-NAT-hyd, which is then translated to a gradual decrease in the H-O-H bond angle from 108.5 to 106.7°. This blue-shift of the H-O-H bending band is suspected to be related to the increase in the bonding behavior of the water molecules in the channel. Kolesov and Geiger reported that the force constant of the bending vibration decrease with an increase in the H-O-H angle (Kolesov and Geiger 2006). However, the frequency of the H-O-H bending band of Li-NAT-hyd (1637 cm^{-1}) is slightly higher than that of Na-NAT-hyd whereas that of K-NAT-hyd (1621 cm^{-1}) is much lower than the corresponding

values of all the other alkali-metal forms. The latter might be attributed to the lower force constant of the bending vibration of water molecules in K-NAT-hyd, thereby enabling K-NAT-hyd higher ion-exchange capacity, compared to the original sodium-form (Lee et al. 2010). On the other hand, the changes in the O-H stretching vibrational modes reveal different arrangements of water molecules along the helical channels. The numbers of the observable O-H stretching vibration bands can be identified to be 2, 2, 2, 3, and 3 for Li-, Na-, K-, Rb-, and Cs-NAT-hyd, respectively. Here, the overlapping IR bands of the O-H stretching vibrations for Rb- and Cs-NAT-hyd were identified by fitting the spectra with a Lorentzian function. For Na-NAT-hyd, two O-H stretching vibration bands are clearly observed as sharp peaks at 3322 and 3538 cm^{-1}, which is consistent with the ordered distribution of water molecules giving rise to two separate OH···O interatomic distances of 2.85 and 3.00 Å (Baur et al. 1990). The band with low intensity at 3220 cm^{-1} (Fig. 3b) represents a Fermi-resonanced double bending mode of water molecules (Kolesov and Geiger 2006). The cation and water distribution in Li-NAT-hyd is similar to that of Na-NAT-hyd, and hence we observe again two O-H stretching vibrational bands at 3338 and 3546.8 cm^{-1}, close to those observed in Na-NAT-hyd (Fig. 3b). On the other hand, K-NAT-hyd and Rb-NAT-hyd exhibit groups of broad peaks (at 3480 and 3579 cm^{-1} and at 3294, 3443, and 3548 cm^{-1}, respectively) merged into a broad band of O-H stretching vibration (Fig. 3b). This is due to the statistical disordering of water molecules along the middle of the helical channels to give rise to closely separated OH···O distances (Lee et al. 2010). Here again, the broad peaks with dashed curves at lower frequency are interpreted as a double bending mode of water molecule (Fig. 3b). It is a well-known fact that the frequency of the O-H stretching vibration is proportional to the OH···O distances and hence inversely proportional to the O-H bond length (Libowitzky 1999). The stretching vibration band at 3579 cm^{-1} in K-NAT-hyd corresponds to a slightly longer OH···O distance than 3.00 Å, which is in good agreement with our previous structural study where we showed water oxygen to framework oxygen distances of 3.09(1) and 3.11(1) Å (Lee et al. 2010). For Cs-NAT-hyd, the observation of three separate O-H stretching vibration bands (3286, 3424, and 3463 cm^{-1}) conforms to the single water site model showing three well-separated water oxygen to framework oxygen distances [2.60(1), 3.07(1), and 3.27(1) Å] (Lee et al. 2010). No apparent O-H vibrational bands are observed in the spectra of Rb-NAT-deh and Cs-NAT-deh, which confirms that these materials indeed exist anhydrous at ambient conditions. Those weak and broad peaks around 3450 cm^{-1} in the spectra of Rb-NAT-deh and Cs-NAT-deh are interpreted to be the effect of the water molecules adsorbed on the particle surfaces.

In summary, we have reported here combined synchrotron IR and micro-Raman spectroscopic characterizations of alkali-metal cation-forms of natrolites both in the hydrated (M-NAT-hyd, M = Li, Na, K, Rb, and Cs) and some stable dehydrated forms (M-NAT-deh, M = Rb and Cs). Our results establish that the red shifts in the frequencies of the helical 8-ring channel as well as the 4-ring unit are sensitive to the structural changes and can be used to distinguish different alkali-metal cation-forms and their hydration status. We have also demonstrated that based on the systematic frequency shifts in the H-O-H bending band and the changes in the O-H stretching vibration modes, the spectroscopic data of the hydrated natrolites can be correlated with the structural models to detail the arrangements and bonding characteristics of the water molecules along the helical channels.

Acknowledgments

This work was supported by the Global Research Lab Program of the Ministry of Education, Science, and Technology (MEST) of the Korean Government. Y. Lee acknowledges the support from the Nuclear R&D Program of the Korea Research Foundation to build the micro-Raman system used in this study. The use of the beamline U2A at NSLS is supported by COMPRES, the Consortium for Materials Properties Research in Earth Sciences under NSF Cooperative Agreement EAR 06-49658 and by the U.S. Department of Energy, Office of Science, Office of Basic Energy Sciences, under Contract No. DE-AC02-98CH10886. Research carried out in part at the NSLS at BNL is supported by the U.S. Department of Energy, Office of Basic Energy Sciences.

References cited

Artioli, G., Smith, J.V., and Kvick, Å. (1984) Neutron diffraction study of natrolite, $Na_2Al_2Si_3O_{10}·2H_2O$, at 20 K. Acta Crystallographica, C40, 1658–1662.

Baur, W.H., Kassner, D., Kim, C.H., and Sieber, N.H.W. (1990) Flexibility and distortion of the framework of natrolite: crystal structures of ion-exchanged natrolites. European Journal of Mineralogy, 2, 761–769.

Boutin, H., Safford, G.J., and Danner, H.R. (1964) Low frequency motions of H_2O molecules in crystals. Journal of Chemical Physics, 40, 2670–2679.

Breck, D.W. (1974) Zeolite Molecular Sieves: Structure, Chemistry, and Use. Wiley, London.

De Man, A.J.M. and van Santen, R.A. (1992) The relation between zeolite framework structure and vibrational spectra. Zeolites, 12, 269–279.

Demontis, P., Gulín-González, J., Dtara, G., and Suffritti, G.B. (2005) Structure and dynamics of hydrogen-bonded water helices in high pressure hydrated phase of natrolite studied by molecular dynamics simulations. Studies in Surface Science and Catalysis, 155, 199–211.

Dutta, P.K., Shieha, D.C., and Puria, M. (1988) Correlation of framework Raman bands of zeolites with structure. Zeolites, 8, 306–309.

Flanigen, E.M., Khatami, H., and Szymanski, A.H. (1971) Infrared Structural Studies of Zeolite Frameworks. Advances in Chemistry, 101, 201–229.

Goryainov, S.V. and Belitsky, I.A. (1995) Raman spectroscopy of water tracer diffusion in zeolite single crystals. Physics and Chemistry of Minerals, 22, 443–452.

Goryainov, S.V. and Smirnov, M.B. (2001) Raman spectra and lattice-dynamical calculations of natrolite. European Journal of Mineralogy, 13, 507–519.

Goryainov, S.V., Smirnov, M.B., and Shebanin, A.P. (2000) Calculation of lattice dynamics of natrolite and its instability under pressure. Doklady Physical Chemistry, 375, 263–267.

Gottardi, G. and Galli, E. (1985) Natural Zeolites. Springer-Verlag, Berlin.

Gunter, M.E. and Ribbe, P.H. (1993) Natrolite group zeolites: Correlations of optical properties and crystal chemistry. Zeolites, 13, 435–440.

Kolesov, B.A. and Geiger, C.A. (2006) Behavior of H_2O molecules in the channels of natrolite and scolecite: A Raman and IR spectroscopic investigation of hydrous microporous silicates. American Mineralogist, 91, 1039–1048.

Kvick, Å., Ståhl, K., and Smith, J.V. (1985) A neutron diffraction study of the bonding of zeolitic water in scolecite at 20 K. Zeitschrift für Kristallographie, 171, 141–154.

Lee, Y., Lee, Y., and Seoung, D. (2010) Natrolite may not be a "soda-stone" any more: part 1.Structural study of fully K-, Rb-, and Cs-exchanged natrolite. American Mineralogist, 95, 1636–1641.

Lee, Y., Seoung, D., Liu, D., Park, M.B., Hong, S.B., Bai, J.M., Kao, C.C., Vogt, T., and Lee, Y. (2011) In-situ dehydration study of fully K-, Rb-, and Cs-exchanged natrolite. American Mineralogist, 96, 393–401.

Line, C.M.B. and Kearley, G.J. (1998) The librational and vibrational spectra of water in natrolite, $Na_2Al_2Si_3O_{10}·2H_2O$ compared with ab-initio calculations. Chemical Physics, 234, 207–222.

Libowitzky, E. (1999) Correlation of O-H Stretching Frequencies and O-H···O Hydrogen Bond Lengths in Minerals. Monatshefte für Chemie, 130, 1047–1059.

Liu, D., Lei, W.W. Liu, Z.X., and Lee, Y. (2010) Spectroscopic study of pressure–induced phase transitions in natrolite. The Journal of Physical Chemistry C, 114, 18819–18824.

Liu, Z., Hu, J., Mao, H.K., and Hemley, R.J. (2002) High-pressure synchrotron x-ray diffraction and infrared microspectroscopy: applications to dense hydrous phases. Journal of Physics: Condensed Matter, 14, 10641–10646.

Meier, W.M. (1960) The crystal structure of natrolite. Zeitschrift für Kristallographie, 113, 430–444.

Pechar, F. and Rykl, D. (1983) Study of the vibrational spectra of natural natrolite. Canadian Mineralogist, 21, 689–695.

Manuscript received July 1, 2011
Manuscript accepted November 1, 2011
Manuscript handled by Aaron Celestian